Rapid Communications

Double quantum dot scenario for spin resonance in current noise

Baruch Horovitz and Anatoly Golub
Department of Physics, Ben Gurion University, Beer Sheva 84105, Israel

(Received 1 April 2019; revised manuscript received 16 June 2019; published 28 June 2019)

We show that interference between parallel currents through two quantum dots, in the presence of spin-orbit interactions and strong on-site Coulomb repulsion, leads to resonances in current noise at the corresponding Larmor frequencies. An additional resonance at the difference of Larmor frequencies is present even without spin-orbit interaction. The resonance lines have strength comparable to the background shot noise and therefore can account for the numerous observations of spin resonance in scanning tunneling microscope noise with nonpolarized leads. We solve also several other models that show similar resonances.

DOI: 10.1103/PhysRevB.99.241407

Coherent control and detection of a single spin are fundamental challenges in nanoscience and nanotechnology, aiming to determine electronic structures as well as provide qubits for quantum information processing [1,2]. Of particular interest are studies that combine the high-energy resolution of electron spin resonance (ESR) with the high spatial resolution of a scanning tunneling microscope (STM). These ESR-STM studies are of two types, either monitoring the current power spectrum in a DC bias [3–5], or monitoring the DC current when an additional AC voltage is tuned to resonance conditions [6–8]. In the latter case with a magnetic tip [7,8] the theory is well understood [7,9]. In Ref. [6] the tip is apparently nonmagnetic, hence it should be interpreted as the inverse phenomenon to that of the first type.

We focus here on the ESR-STM phenomenon of the first type, i.e., a DC bias alone. The experimental technique is conceptually simple: an STM tip is placed above a localized spin center in the presence of a DC magnetic field and the power spectrum, monitoring the current fluctuations, is measured; the data exhibits a sharp resonance at the expected Larmor frequency [3–5] even at room temperature. This phenomena has been further confirmed by an associated electron-nuclear double resonance effect [10]. The understanding of this ESR-STM phenomenon presents a theoretical challenge even at present [4]. It was proposed early on that a spin-orbit coupling is essential for converting the spin fluctuations to current noise, assuming also that the tip and substrate are spin polarized [11–13]. However, the experimental data [3–5] involves nonpolarized tip and substrate. It was argued that an effective spin polarization is realized either as a fluctuation effect [5,14] or due to $1/f$ magnetic noise of the tunneling current [15]. The first theoretical model that conclusively showed an ESR-STM phenomena in this case, i.e., nonpolarized electrodes in a DC setup, was a nanoscopic interferometer model [16,17]. In this model the current has an additional channel of direct tunneling from the tip to the substrate in parallel to the current via the spin states. The interference between the two channels leads to an ESR resonance; however, the signal is rather weak. Furthermore this model ignores on-site Coulomb interactions, that are expected to be significant at a localized spin site.

In the present work we propose a mechanism for the ESR-STM phenomenon, a mechanism that provides a strong signal, comparable to that of the background shot noise, and allows for a strong Coulomb interaction at the spin site. The model assumes the presence of an additional spin such that the current passes in parallel via two spins, i.e., a double quantum dot (DQD). The additional spin is unintentional in the ESR-STM experiments so far, yet its presence can be tested by monitoring our predictions. In particular, in addition to the expected resonance at $\nu_1 = g_1\mu_B H$ additional resonances are present at $g_2\mu_B H$ and at $|g_1 - g_2|\mu_B H$; g_1, g_2 are the g factors of the two spins, respectively, μ_B is the Bohr magneton, and H is the DC magnetic field. We solve also the single spin model [16,17] with strong on-site Coulomb repulsion, as well as the noninteracting two-spin model. We find that the DQD model provides a strong signal-to-noise ratio and is most likely to account for the ESR-STM data. The properties of all the studied models are summarized in Table I below.

We review first the previous model [16,17] that involves interference between tunneling via the spin and direct tunneling, as illustrated in Fig. 1(a). Consider $l = L, R$ (left, right) fermion leads (i.e., tip and substrate) with the Hamiltonian $\mathcal{H}_0 = \sum_{l,k,\sigma} \epsilon_{lk} c^\dagger_{lk\sigma} c_{lk\sigma}$ where $\sigma = \pm$ denotes the spin and k are continuum states; $c_{lk\sigma}$ are the lead fermion operators whose dispersions ϵ_{lk} include the voltage and are spin independent, justified by the small ratio 10^{-5} of the Larmor frequency and a typical electron bandwidth. The spin site involves fermion operators d_σ and a Hamiltonian $\mathcal{H}_d = \sum_\sigma (\epsilon_0 + \frac{1}{2}\nu\sigma) d^\dagger_\sigma d_\sigma$ where $\nu = g\mu_B H$ is the (single) Larmor frequency with g factor g. The reservoirs are connected by a direct tunneling as well as by tunneling via the spin; the latter allows for an SU(2) spin-orbit rotation [16,17] $\hat{u} = e^{i\sigma_z\phi} e^{(1/2)i\sigma_y\theta}$ where $\boldsymbol{\sigma}$ are the Pauli matrices. The total Hamiltonian is $\mathcal{H}_1 = \mathcal{H}_0 + \mathcal{H}_d + \mathcal{H}^{(1)}_{\rm tun}$ with the tunneling term,

$$\mathcal{H}^{(1)}_{\rm tun} = t c^\dagger_L d + t' c^\dagger_R \hat{u} d + W c^\dagger_L c_R + \text{H.c.}, \tag{1}$$

where all operators are now spinors and $c^\dagger_l = \sum_k c^\dagger_{lk}$ is at the tunneling site. The current noise for this model has been solved exactly [16,17] with results summarized in the first column of Table I, yet it is instructive to derive the

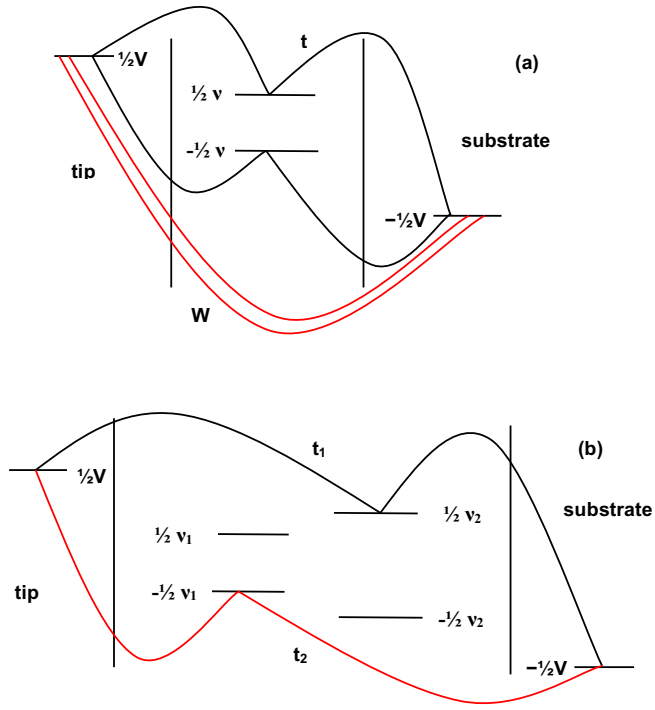

FIG. 1. Interference paths that lead to an ESR-STM effect: (a) paths via a single spin and a direct tunneling path and (b) paths via two spins in parallel (for $\Delta = 0$).

main results heuristically. The resonance linewidth is seen from a Golden rule $\Gamma = 2\pi t^2 N(0)$, assuming now $t = t'$ and the density of states $N(0)$ per spin of both leads are taken equal, for simplicity. The resonance in the current correlation involves a closed loop with a given spin that passes at both spin levels, as illustrated in Fig. 1(a). Hence one needs at least six tunneling events: four via the spin and two direct tunnelings, as well as two spin flips of probability $\sin^2\frac{1}{2}\theta$, hence an amplitude $\sim t^4 W^2 \sin^2\frac{1}{2}\theta$ which multiplies a Lorentzian of width Γ, hence the peak amplitude is $\sim t^4 W^2 \sin^2\frac{1}{2}\theta/\Gamma \sim t^2 W^2 \sin^2\frac{1}{2}\theta$. This derivation is valid if the spin levels are within the voltage window [16,17], i.e., $|\epsilon_0| < \frac{1}{2}eV[1 + O(T/eV)]$ at temperature T. The direct current $L \to R$ is also found by a golden rule rate $2\pi W^2 N(0)$ per spin times the final number of available states eV, i.e., $J_W = 4\pi e^2 V W^2 N^2(0)$. Assuming $W \gg t$ the background shot noise is $2eJ_W$, hence the Fano factor, i.e., the ratio of the resonance peak to that of the background, is $F \approx \Gamma \sin^2\frac{1}{2}\theta/eV$. For [4,5] $\Gamma \approx 10$ MHz, $V \approx 1$ eV this ratio is $\approx 10^{-6}$, too small to account for ESR-STM data. [If $t \gg W$, the Fano factor would be even smaller, $F \sim W^2 N^2(0)$.]

We consider next our new model; first, its noninteracting variant. The model involves current transport via two spins, in parallel, i.e., the Hamiltonian is $\mathcal{H}_2 = \mathcal{H}_0 + \mathcal{H}_d^{(2)} + \mathcal{H}_{\rm tun}^{(2)}$ where d_1, d_2 are fermion spinor operators on the two spin sites,

$$\mathcal{H}_d^{(2)} = \tfrac{1}{2}\nu_1 d_1^\dagger \sigma_z d_1 + d_2^\dagger\big(\Delta + \tfrac{1}{2}\nu_2\sigma_z\big)d_2,$$
$$\mathcal{H}_{\rm tun}^{(2)} = c_L^\dagger[t_1 d_1 + t_2 d_2] + c_R^\dagger[t_1' d_1 + t_2'\hat{u} d_2]. \qquad (2)$$

We assume that only the R electrode (probably the tip) has significant spin-orbit interaction. In general this yields two SU(2) spin rotation matrices $\hat{u}_1, \hat{u}_2$ for tunneling from R to sites 1 and 2, respectively, i.e., $t_1' c_R^\dagger \hat{u}_1 d_1 + t_2' c_R^\dagger \hat{u}_2 d_2$. In general the wave functions of the two spins differ in their orbital part as well as in their locations, hence we expect $\hat{u}_1 \neq \hat{u}_2$. In the Supplemental Material [18] we extend Bardeen's formula to include spin-orbit coupling and estimate the spin-flip angle θ. We find that $0 < |\tan\frac{1}{2}\theta| \lesssim 1$, depending on the location of the spin site. Hence two spin locations can lead to fairly different $\hat{u}_1, u_2$. We then rotate $c_R^\dagger \to c_R^\dagger \hat{u}_1^\dagger$ so as to cancel $\hat{u}_1$ in the d_1 term while $\hat{u} = \hat{u}_1^\dagger \hat{u}_2$ for the d_2 term, resulting in Eq. (2).

The current fluctuations correspond now to Fig. 1(b), i.e., a closed loop passing through both spins, at either level of each spin. A resonance appears then at the difference in energy levels, i.e., at $\frac{1}{2}|\nu_1 \pm \nu_2|$; the $+(-)$ sign is for trajectories through opposite (same) side levels. For a finite relative chemical potential Δ there are more resonance lines at $|\frac{1}{2}\nu_1 \pm \frac{1}{2}\nu_2 \pm \Delta|$. The significant virtue of the process in Fig. 1(b) is that only four tunneling events are needed, hence a much stronger resonance. We present [18] an exact solution of Eq. (2) with numerical plots of typical results. The solution can be expanded for weak tunneling, with results summarized in the third column of Table I. While the Fano factor is strong the model is inadequate since it neglects on-site Coulomb interactions, expected to be strong for the experimental realizations. Furthermore, the resonance frequencies depend on the unknown Δ parameter. In fact, the addition of Coulomb interactions is essential for confining the dots as neutral so that the chemical potential Δ becomes irrelevant.

TABLE I. Summary of four models for weak tunneling, $\Gamma \ll \nu \ll eV$, and equal tunneling amplitudes t (noninteracting models). The Aharononv-Bohm phase χ is finite only in the second column. The Fano factors in the third column correspond to $|\frac{1}{2}\nu_1 + \frac{1}{2}\nu_2 \pm \Delta|$ and $|\frac{1}{2}\nu_1 - \frac{1}{2}\nu_2 \pm \Delta|$, respectively. In the fourth column the linewidth for $|\nu_1 - \nu_2|$ differs [given by Eq. (8)]. The Fano factor in column 1 or 2 is shown for $W \gg t$ or $W \gg J$, respectively (the correction is shown in the DC current). The Fano factor in column 4 is shown for the ν_1, ν_2 resonances; other cases are in Eq. (9).

	Single spin + direct tunneling		Two spins	
	Noninteracting	Strongly interacting	Noninteracting	Strongly interacting (DQD)
Linewidth Γ	$2\pi t^2 N(0)$	$16\pi J^2 N^2(0) eV$	$4\pi t^2 N(0)$	$16\pi(J_1^2+J_2^2)N^2(0)eV$
DC current	$4\pi e^2 V W^2 N^2(0) + 2e\Gamma$	$2\pi e^2 V(2W^2+3J^2)N^2(0)$	$2e\Gamma$	$\frac{3}{8}e\Gamma$
Resonance frequencies	ν	$\nu+\delta\nu$ and 0	$\lvert\frac{1}{2}\nu_1 \pm \frac{1}{2}\nu_2 \pm \Delta\rvert$	ν_1, ν_2, $\lvert\nu_1-\nu_2\rvert$, 0
Fano factors F	$\frac{3\pi\Gamma}{16eV}\sin^2\frac{1}{2}\theta$	$\sin^2\chi\sin^2\frac{1}{2}\theta$ and $2\sin^2\chi\sin^2\phi\cos^2\frac{1}{2}\theta$	$\frac{1}{8}\sin^2\frac{1}{2}\theta$ and $\frac{1}{8}(1+\cos^2\frac{1}{2}\theta - 2\cos\phi\cos\frac{1}{2}\theta)$	$\frac{2\pi J_1^2 J_2^2}{3(J_1^2+J_2^2)^2}\sin^2\frac{1}{2}\theta$

We proceed now to solve both models, Eqs. (1) and (2), when strong on-site Coulomb interactions are present, as indeed is the case in atoms and small molecules. Considering first Eq. (1), we add a term $Un_\uparrow n_\downarrow$ where $n_\sigma = d_\sigma^\dagger d_\sigma$. The effective Hamiltonian for large U, $-\epsilon_0 \gg t, \nu$ is well known from a Schrieffer-Wolff (SW) transformation [19]

$$\mathcal{H}_1^c = \mathcal{H}_0 + [2Jc_R^\dagger \boldsymbol{\sigma} c_L \cdot \mathbf{S} + We^{-i\chi} c_R^\dagger \hat{u}^\dagger c_L + \text{H.c.}] + \nu S_z, \tag{3}$$

where $\mathbf{S}$ is the spin operator, $J = O(\frac{tt'}{U}, \frac{tt'}{|\epsilon_0|})$, and an Aharonov-Bohm phase χ is introduced, useful in the following. W may include potential scattering terms generated by the SW transformation. We note that J is reduced by the strong Coulomb interaction, i.e., large U and $-\epsilon_0$, an effect known as the Coulomb blockade. We keep in Eq. (3) only exchange terms that allow transport between the electrodes; other exchange terms that involve electrons only on one electrode are neglected since their contribution to transport would be of higher order. We perform [18] a perturbation expansion to order J^2W^2 using the Keldysh method. The result shows, surprisingly, that the resonance term precisely vanishes when $\chi = 0$. In ESR-STM experiments we expect $\chi = 0$ since the nanometric dimensions of the setup allow only a negligible magnetic flux. To motivate this result, consider an interference along the loop $R \to$ (via spin) $\to L \to R$ and an additional trajectory of going around the loop in the opposite direction $R \to L \to$ (via spin) $\to R$. When $\chi = 0$ these trajectories are related by time reversal; the single spin in the loop then yields a relative minus sign, i.e., cancellation. More specifically, these two processes, when the localized spin is flipped up, sum up to

$$\begin{aligned}
&\langle c_L^\dagger \sigma_- c_R c_R^\dagger \hat{u}^\dagger c_L\rangle e^{-i\chi} + \langle c_L^\dagger \hat{u} c_R c_R^\dagger \sigma_- c_L\rangle e^{i\chi} \\
&\quad = f_L(\epsilon_L)[1 - f_R(\epsilon_R)]\{\text{Tr}[\sigma_- \hat{u}^\dagger]e^{-i\chi} + \text{Tr}[\sigma_- \hat{u}]e^{i\chi}\} \\
&\quad = f_L(\epsilon_L)[1 - f_R(\epsilon_R)]2i \sin\chi \sin\tfrac{1}{2}\theta e^{i\phi},
\end{aligned} \tag{4}$$

where $f_l(\epsilon)$ are Fermi functions and $\text{Tr}[\sigma_- \hat{u}^\dagger] = -\text{Tr}[\sigma_- \hat{u}] = 2\sin\frac{1}{2}\theta e^{i\phi}$. Hence the interference cancels at $\chi = 0$. Energy conservation implies $\epsilon_L = \epsilon_R + O(\nu)$ and integration on ϵ_L yields then an eV factor. Additional interference cycles that start at L involving $f_R(\epsilon)[1 - f_L(\epsilon)]$ are negligible for $V > 0$ and $eV \gg \nu, T$. The result (4) is confirmed by detailed perturbation expansion [18], as summarized in the second column of Table I. Hence for the experimentally relevant case with $\chi = 0$ this model may give a resonance only at orders higher than J^2W^2 and therefore does not account for ESR-STM data. We note also that replacing $\sigma_- \to \sigma_z$ in Eq. (4) yields a resonance at $\omega = 0$ with amplitude $\sim \text{Tr}[\sigma_z \hat{u}^\dagger]e^{-i\chi} + \text{Tr}[\sigma_z \hat{u}]e^{i\chi} = 4\sin\chi \sin\phi \cos\frac{1}{2}\theta$.

For completeness, we evaluate the resonance linewidth, relevant when $\chi \neq 0$. The simplest approach is a golden rule for the decay of a spin up by passing an electron from L to R,

$$\begin{aligned}
\Gamma_\downarrow &= 2\pi N^2(0) \int_{\epsilon_L,\epsilon_R} |4J\langle\uparrow|c_{L\downarrow}^\dagger c_{R\uparrow} S_+|\downarrow\rangle|^2 \delta(\epsilon_L - \epsilon_R - \nu) \\
&= 8\pi eVJ^2N^2(0).
\end{aligned} \tag{5}$$

Similarly for $\Gamma_\uparrow$, leading to $\frac{1}{T_1} = \Gamma_\downarrow + \Gamma_\uparrow = 16\pi eVJ^2N^2(0)$, hence for the isotropic interaction in Eq. (3) the linewidth is $1/T_1 = 1/T_2$. This result is confirmed by solving a Lindblad-type equation [18] for the spin dynamics; it is also consistent with the linewidth as derived by higher orders in Keldysh diagrams [20]; however, the framework of the Lindblad equation, being a proper second-order perturbation, is considerably more convenient. The Lindblad equation also shows a shift in the resonance frequency $\delta\nu = -4\pi eVJWN^2(0)\sin\phi\cos\frac{1}{2}\theta\cos\chi$, that may well be larger than the linewidth.

We proceed to our most interesting model, the DQD model with strong on-site Coulomb interactions. Proceeding with a SW-type derivation [18] we find that Eq. (2) is replaced by

$$\begin{aligned}
\mathcal{H}_2^c = \mathcal{H}_0 &+ 2J_1 c_R^\dagger \boldsymbol{\sigma} c_L \cdot \mathbf{S}_1 + 2J_2 c_R^\dagger \hat{u}\boldsymbol{\sigma} c_L \cdot \mathbf{S}_2 \\
&+ \nu_1 S_{1z} + \nu_2 S_{2z},
\end{aligned} \tag{6}$$

which is an obvious extension of the single spin case. This Hamiltonian neglects potential scattering terms that may generate terms beyond those that we study of order $J_1^2 J_2^2$; also $\chi = 0$ here, for simplicity. Tunneling between the two spin sites is neglected, leading to higher order terms for transport [18]; this tunneling yields also a direct exchange between the spins which shifts the Larmor frequencies; we neglect here this effect (e.g., if one spin is on the tip and the other on the surface this exchange is much weaker than either J_1 or J_2).

We note that the spin-orbit factor $\hat{u}$ is essential for observing a resonance at a Larmor frequency. If $\hat{u} = 1$, then the tunneling elements conserve the total spin, while the S_z terms in $\mathcal{H}_2^c$ allow conservation of the z component of the total spin. Thus a closed loop of a lead electron returning to its original spin cannot flip a single spin, i.e., no resonance at either ν_1 or ν_2. The loop can, however, flip both spins in opposite ways, hence a resonance at $|\nu_1 - \nu_2|$ is possible even without spin-orbit effects. In fact, the same symmetry reasoning applies to all the models considered above. We further note that models with transport via a single spin, even if including spin-orbit interaction, e.g., Eq. (6) with $J_1 = 0$, do not show an ESR-STM phenomenon. This is seen by rotating $c_R^\dagger \to c_R^\dagger \hat{u}^\dagger$ so that $\hat{u}$ is canceled and then total S_z conservation rules out a spin-flip resonance. This conclusion holds for models with other types of isotropic exchange interactions [5,14], interactions that commute with the total S_z.

To appreciate the type of results, we consider the loops as in Eq. (4), which for a single spin flip involve σ_- on one spin while σ_z on the other, hence

$$\begin{aligned}
&\langle c_L^\dagger \sigma_- c_R c_R^\dagger \hat{u}\sigma_z c_L\rangle + \langle c_L^\dagger \sigma_z \hat{u}^\dagger c_R c_R^\dagger \sigma_- c_L\rangle \\
&\quad = f_L(\epsilon_L)[1 - f_R(\epsilon_R)]\{\text{Tr}[\sigma_- \hat{u}\sigma_z] + \text{Tr}[\sigma_z \hat{u}^\dagger \sigma_-]\} \\
&\quad = -2f_L(\epsilon_L)[1 - f_R(\epsilon_R)]\sin\tfrac{1}{2}\theta e^{i\phi}.
\end{aligned} \tag{7}$$

Hence we expect resonances of the form $\sim J_1^2 J_2^2 \sin^2\frac{1}{2}\theta\delta(\omega - \nu_i)$, $i = 1, 2$. An additional resonance at $|\nu_1 - \nu_2|$ appears when $\sigma_z \to \sigma_+$ in Eq. (7); the matrix elements then lead to $2\cos\frac{1}{2}\theta e^{i\phi}$, hence a resonance $\sim J_1^2 J_2^2 \cos^2\frac{1}{2}\theta\delta(\omega - |\nu_1 - \nu_2|)$. One further resonance is possible at $\omega = 0$ when $\sigma_- \to \sigma_z$ in Eq. (7), i.e., no spin flips, leading to $4\cos\phi\cos\frac{1}{2}\theta$, hence a resonance $\sim J_1^2 J_2^2 \cos^2\phi\cos^2\frac{1}{2}\theta\delta(\omega)$. Finally, there is no resonance at $\nu_1 + \nu_2$ since $\sigma_-^2 = 0$.

We proceed now to our diagrammatic expansion. First, consider skeleton diagrams, i.e., without Keldysh indices, that show readily which type of diagrams to fourth order can

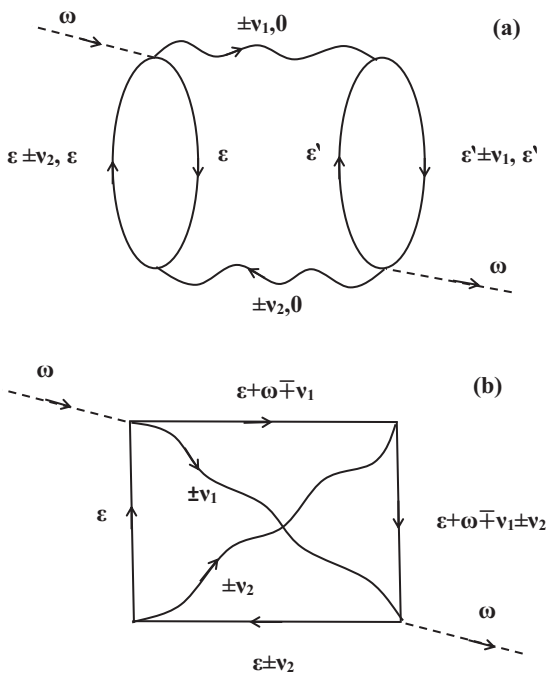

FIG. 2. Skeleton diagrams: solid straight lines are electron propagators on either the right or the left electrode (being interchanged at each vertex), wavy lines represent spin propagator with poles at the Larmor frequency ν_1 or ν_2 or at 0 (S_z propagator), and dashed lines are external current sources. (a) Conservation of frequency at either current vertex leads to resonances $\delta(\omega \mp \nu_1)$, $\delta(\omega \mp \nu_2)$, $\delta(\omega \mp |\nu_1 - \nu_2|)$, and $\delta(\omega)$. (b) A diagram that does not show a resonance.

produce a resonance. Figure 2(a) shows a typical diagram that has a resonance, i.e., frequency conservation at each vertex yields readily δ function resonances at ν_1, ν_2, $|\nu_1 - \nu_2|$, and 0. In contrast, Fig. 2(b) shows that all spin frequencies merely shift an electron energy which is being integrated. Hence a weak ω dependence, i.e., a nonresonant effect. [We note that similar skeleton diagrams can be constructed also for our single dot model, Eq. (3); one spin line is eliminated while its vertices remain as the direct tunneling W term.]

We present a detailed Keldysh diagrammatic expansion [18]. The results are consistent with the reasoning above and are summarized in the fourth column of Table I. We also solve [18] a Lindblad equation for this case to identify the various linewidths $\Gamma(\omega_{\rm res})$ of the various resonances $\omega_{\rm res}$, leading to

$$\Gamma = 16\pi eVN^2(0)\left(J_1^2 + J_2^2\right), \quad \omega_{\rm res} = \nu_1,\ \nu_2,\ 0,$$
$$\Gamma(|\nu_1 - \nu_2|) = 16\pi eVN^2(0)\left(J_1^2 + J_2^2 - 2J_1J_2\cos\tfrac{1}{2}\theta\cos\phi\right). \tag{8}$$

This result is similar to that of the single spin case obtained from Eq. (5), except that each spin is affected also by the longitudinal relaxation of the other spin; furthermore, the $\nu_1 - \nu_2$ resonance includes a nonsecular $\sim J_1J_2$ term [18].

The DC current is given in Table I; as expected it is $\approx e\Gamma$, so that the background shot noise is $\approx e^2\Gamma$. The resonance signal at maximum is obtained from the discussion following Eq. (7) and is confirmed by the diagrammatic expansion [18], with the replacement $\delta(\omega - \omega_{\rm res}) \to 1/\pi\,\Gamma(\omega_{\rm res})$. The ratio of this peak value and that of the background is given for ν_1, ν_2 in the table while for the other resonances it is $F(\omega_{\rm res})$,

$$F(0) = \frac{4\pi J_1^2J_2^2}{3\left(J_1^2 + J_2^2\right)^2}\cos^2\tfrac{1}{2}\theta\cos^2\phi,$$
$$F(|\nu_1 - \nu_2|) = \frac{2\pi J_1^2J_2^2\cos^2\frac{1}{2}\theta\left(2 + \tanh\frac{\nu_1}{2T}\tanh\frac{\nu_2}{2T}\right)}{3\left(J_1^2 + J_2^2\right)\left(J_1^2 + J_2^2 - 2J_1J_2\cos\theta\,\cos\phi\right)}. \tag{9}$$

It is remarkable that the resonance at $|\nu_1 - \nu_2|$ is strongest without spin-orbit coupling, i.e., $\theta = \phi = 0$, with a narrow linewidth $\sim(J_1 - J_2)^2$.

We consider next the relevance of our results to the experimental situation [3–5]. First, we note that the data shows a sharp resonance even at room temperature. This is fully consistent with our results since the linewidth is dominated by the voltage with $eV \gg k_BT$. Second, we note that the linewidth of 25 MHz at $I = 0.1$ nA [10] implies that the DC current via the spins (Table I) is $\frac{3}{8}e\Gamma \approx 10^{-4}$ nA, much smaller than the total current. We expect then that most of the current tunnels directly between the tip and substrate, indeed a dominant tunneling as it is not Coulomb blockaded. We expect that this current is incoherent with those via the spins, otherwise it would lead to a large shift $\delta\nu$ in the resonance frequency [see paragraph below Eq. (5)]. Finally, the ratio of peak noise power to that of the shot noise has been estimated [5] as $O(1)$; however, since the power spectrum is measured via modulation of the magnetic field its absolute value has not been so far directly measured.

These experiments [3–5] aim to probe a known spin site on a surface. We propose that a second spin is present, allowing for the observed strong signal. The most likely location for the second spin is on the STM tip, which is usually made of a heavy metal with significant spin-orbit coupling. Indeed, the presence of dangling bond surface states in various tip materials is known [21]; such states are candidates for spin sites. By extending the measured frequency range, we predict the observation of a second Larmor frequency ν_2 as well as a signal at a lower frequency $|\nu_1 - \nu_2|$. The latter in fact may well be stronger than those at either ν_1 or ν_2 if the spin-orbit effect is weak, i.e., small θ. We note that preliminary data shows a strong signal at low frequency for either defects on a SiC surface or for Tempo molecules on Au substrate [22].

We note finally that the second type of ESR-STM, i.e., enhanced DC current at resonance with an applied AC voltage [7,8], involves a magnetized Fe atom on the tip. While this is superficially similar to our two-spin scenario, it is a fundamentally different mechanism, being based on a permanently strong magnetic atom. In our scenario both spin sites exhibit spin fluctuations; in fact, even the average spin of each site is extremely weak [18], $\approx\nu_i/eV \ll 1$ ($i = 1, 2$); yet, data on noise in the spin current might show similarities.

In conclusion we have solved a number of models showing an ESR-STM phenomenon, concluding that the model of two spins with strong on-site Coulomb interactions is the most likely to account for the data. Observation of our prediction for additional magnetic-field-dependent frequencies in the power spectrum would be the clearest support for our mechanism.

We thank Y. Manassen for illuminating discussions on his data and the experimental setup. We also thank C. P. Moca, G. Zaránd, and Y. Meir for stimulating discussions. B.H. also gratefully acknowledges funding by the German DFG through the DIP programme (FO703/2-1).

[1] F. H. L. Koppens, C. Buizert, K. J. Tielrooij, I. T. Vink, K. C. Nowack, T. Meunier, L. P. Kouwenhoven, and L. M. K. Vandersypen, Nature (London) **442**, 766 (2006).
[2] D. D. Awschalom, L. C. Bassett, A. S. Dzurak, E. L. Hu, and J. R. Petta, Science **339**, 1174 (2013).
[3] Y. Manassen, R. J. Hamers, J. E. Demuth, and A. J. Castellano, Jr., Phys Rev. Lett. **62**, 2531 (1989).
[4] For a review, see A. V. Balatsky, M. Nishijima, and Y. Manassen, Adv. Phys. **61**, 117 (2012).
[5] Y. Manassen, M. Averbukh, and M. Morgenstern, Surf. Sci. **623**, 47 (2014).
[6] S. Müllegger, S. Tebi, A. K. Das, W. Schöfberger, F. Faschinger, and R. Koch, Phys. Rev. Lett **113**, 133001 (2014).
[7] S. Baumann, W. Paul, T. Choi, C. P. Lutz, A. Ardavan, and A. J. Heinrich, Science **350**, 417 (2015).
[8] P. Willke, W. Paul, F. D. Natterer, K. Yang, Y. Bae, T. Choi, J. Fernández-Rossier, A. J. Heinrich, and C. P. Lutz, Sci. Adv. **4**, eaaq1543 (2018).
[9] G. Shavit, B. Horovitz, and M. Goldstein, Phys. Rev. B **99**, 195433 (2019).
[10] Y. Manassen, M. Averbukh, M. Jbara, B. Siebenhofer, A. Shnirman, and B. Horovitz, J. Magn. Reson. **289**, 107 (2018).
[11] L. N. Bulaevskii, M. Hruska, and G. Ortiz, Phys. Rev. B **68**, 125415 (2003).
[12] S. A. Gurvitz, D. Mozyrsky, and G. P. Berman, Phys. Rev. B **72**, 205341 (2005).
[13] M. Braun, J. König, and J. Martinek, Phys. Rev. B **74**, 075328 (2006).
[14] A. V. Balatsky, Y. Manassen, and R. Salem, Philos. Mag. B **82**, 1291 (2002); Phys. Rev. B **66**, 195416 (2002).
[15] Y. Manassen and A. V. Balatsky, Isr. J. Chem. **44**, 401 (2004).
[16] A. Caso, B. Horovitz, and L. Arrachea, Phys. Rev. B **89**, 075412 (2014).
[17] A. Golub and B. Horovitz, Phys. Rev. B **88**, 115423 (2013).
[18] See Supplemental Material at http://link.aps.org/supplemental/10.1103/PhysRevB.99.241407 for details on tunneling in presence of spin-orbit interaction, Schrieffer-Wolff transformation, current noise for various models using Keldysh diagrams and resonance linewidth using the Lindblad method, which includes Refs. [19,23–33].
[19] A. C. Hewson, *The Kondo Problem to Heavy Fermions* (Cambridge University Press, Cambridge, UK, 1993).
[20] J. Paaske, A. Rosch, J. Kroha, and P. Wölfle, Phys. Rev. B **70**, 155301 (2004).
[21] C. J. Chen, Phys. Rev. Lett. **65**, 448 (1990); Phys. Rev. B **42**, 8841 (1990).
[22] Y. Manassen (private communication).
[23] J. Bardeen, Phys. Rev. Lett. **6**, 57 (1961).
[24] M. Devel, C. Girard, and C. Joachim, Phys. Rev. B **53**, 13159 (1996).
[25] A. M. Shikin, A. Varykhalov, G. V. Prudnikova, D. Usachev, V. K. Adamchuk, Y. Yamada, J. Riley, and O. Rader, Phys. Rev. Lett. **100**, 057601 (2008).
[26] E. Rotenberg, J. W. Chung, and S. D. Kevan, Phys. Rev. Lett. **82**, 4066 (1999).
[27] A. Kamenev and A. Levchenko, Adv. Phys. **58**, 197 (2009).
[28] A. A. Abrikosov, Phys. Physique Fiz. **2**, 5 (1965).
[29] C. P. Moca, P. Simon, C.-H. Chung, and G. Zaránd, Phys. Rev. B **89**, 155138 (2014).
[30] A. Shnirman and I. Kamleitner, Physics of Quantum Information, Lecture notes (unpublished).
[31] M. Schlosshauer, *Decoherence and the Quantum-to-Classical Transition* (Springer, New York, 2007), Chap. 4.
[32] A. Rosch, J. Kroha, and P. Wölfle, Phys. Rev. Lett. **87**, 156802 (2001).
[33] O. Parcollet and C. Hooley, Phys. Rev. B **66**, 085315 (2002).